

***Ab initio* nonadiabatic study of the $3p\pi D^1\Pi_u^+$ state of H_2 and D_2** M. Glass-Maujean,¹ H. Schmoranzner,² Ch. Jungen,^{3,4} I. Haar,⁵ A. Knie,⁵ P. Reiss,⁵ and A. Ehresmann⁵¹*Laboratoire de Physique Moléculaire pour l'Atmosphère et l'Astrophysique, UMR 7092 UPMC/CNRS, Université Pierre et Marie Curie, 4 place Jussieu, 75252 Paris Cedex 05, France*²*Fachbereich Physik, Technische Universität Kaiserslautern, D-67653 Kaiserslautern, Germany*³*Laboratoire Aimé Cotton du CNRS, Bâtiment 505, Université de Paris-Sud, F-91405 Orsay, France*⁴*Department of Physics and Astronomy, University College London, London WC1E 6BT, United Kingdom*⁵*Institute of Physics and Interdisciplinary Nanostructure Science and Technology, Heinrich-Plett-Strasse 40, Universität Kassel, D-34132 Kassel, Germany*

(Received 12 July 2012; published 15 November 2012)

We present nonadiabatic, fully *ab initio*, systematic calculations of the $3p\pi D^1\Pi_u^+$ level energies, Λ doublings, and absorption line intensities and widths for H_2 and D_2 even for those levels that are strongly predissociated. The multichannel quantum defect theory calculations are based on the latest quantum-chemical clamped-nuclei data of Wolniewicz and collaborators [L. Wolniewicz and G. Staszewska, *J. Mol. Spectrosc.* **220**, 45 (2003); G. Staszewska and L. Wolniewicz, *ibid.* **212**, 208 (2002)]. The theoretical values are compared with previously published data [G. D. Dickenson, T. I. Ivanov, M. Roudjane, N. de Oliveira, D. Joyeux, L. Nahon, W.-Ü. L. Tchang-Brillet, M. Glass-Maujean, I. Haar, A. Ehresmann, and W. Ubachs, *J. Chem. Phys.* **133**, 144317 (2010); G. D. Dickenson, T. I. Ivanov, W. Ubachs, M. Roudjane, N. de Oliveira, D. Joyeux, L. Nahon, W.-Ü. L. Tchang-Brillet, M. Glass-Maujean, H. Schmoranzner, A. Knie, S. Kübler, and A. Ehresmann, *Mol. Phys.* **109**, 2693 (2011)] and with absolute line intensity measurements. The overall agreement is very good. The enhanced precision of the calculations leads to additional assignments and to several corrections of previous literature data.

DOI: 10.1103/PhysRevA.86.052507

PACS number(s): 33.70.Jg, 33.70.Fd, 33.80.Gj, 33.20.Ni

I. INTRODUCTION

The $3p\pi D^1\Pi_u$ state of H_2 , first observed in the absorption spectrum in the 1930s [1], has been the subject of numerous experimental [2–8] and theoretical studies [9–14]. The $^1\Pi^+$ component for the levels with $v \geq 3$ undergoes a very rapid predissociation inducing typical Beutler-Fano profiles of the absorption lines [15,16]. In contrast, the $^1\Pi^-$ component is long-lived, leading to vacuum-ultraviolet (VUV) emissions at energies far higher than the ionization and dissociation thresholds [13,14,17,18].

Recently, the $^1\Pi^-$ level energies were calculated very precisely using two different *ab initio* approaches—coupled equations (CEs) and multichannel quantum defect theory (MQDT) [19]—whereas the $^1\Pi^+$ level energies did not receive the same attention. They have been calculated by CEs only for the lower unpredissociated levels ($v < 3$); the fast predissociation makes the CE calculations unstable and unreliable [20]. The MQDT approach may overcome this difficulty [11].

The spectacular predissociation is due to nonadiabatic couplings, typically the Coriolis coupling with the $3p\sigma B'^1\Sigma_u^+$ state. The predissociation widths were first calculated in the 1970s [9,10]. In these calculations, the system was considered to be a two-state problem involving the B' and D states, and the potential curves used were Rydberg-Klein-Rees (RKR) curves. The same simple approach was applied later on in Refs. [21,22], using more precise *ab initio* potential curves, to reproduce the global behavior of the dissociation widths of the vibrational progression. More elaborate *ab initio* CE calculations have been performed considering three coupled states, namely the B , B' , and D states [23,24]. In 1984, Jungen [25] showed that the MQDT approach could be extended to include predissociation, and the widths of

the $D^1\Pi^+$ levels were chosen to test the various theoretical sophistications [11,12].

Recently, precise measurements of the energies of these levels have been published for both isotopes H_2 [21] and D_2 [22], including the intensities of the absorption lines of D_2 . These experimental data will be compared with the theoretical values presented herein. The H_2 line intensities used for comparison are additional experimental data.

The present work is part of an effort to provide a coherent and systematic experimental and theoretical account of the absorption spectrum of diatomic hydrogen and its isotopomers up to the $H(1s) + H(n = 4)$ dissociation limit [13,14,26–28]. In addition to reporting a fully *ab initio* nonadiabatic MQDT calculation of the $3p\pi D^1\Pi_u^+$ energy levels, Λ doublings, and line intensities and widths, based on the latest quantum-chemical clamped-nuclei calculations of Wolniewicz and collaborators [29], the present paper contains measurements of absolute line intensities with greater accuracy than those reported previously in Ref. [8].

II. THEORETICAL APPROACH

Accurate *ab initio* calculations of level energies in excited electronic states of diatomic molecules are known to be difficult. There are currently two theoretical approaches available that are capable of taking into account nonadiabatic interactions. Both approaches have been pioneered in applications to excited states of H_2 in the 1970s [30,31]. The first one was based on frame transformation MQDT combined with *ab initio* potential energy curves. The second one evaluated nonadiabatic interactions by solving coupled differential equations for the nuclear motion in mixed electronic states. These calculations were also based on *ab initio* electronic

potential energy curves, which were combined with nuclear kinetic operator coupling functions, also evaluated from first principles.

The $3p\pi D^1\Pi_u^+ J=2$ levels ($3 \leq v \leq 11$) of H_2 have been investigated by one of the first MQDT approaches [30], and then by a MQDT approach combined with a noniterative eigenchannel R -matrix method [11]; these calculations were not *ab initio*. Later on, a more sophisticated MQDT treatment taking into account simultaneously dissociation and ionization was demonstrated in a short energy range of the H_2 absorption spectrum including the $R(1) 3p\pi D v=8 - X, v''=0$ line [12]. Recently, accurate CE calculations have been performed of the $D^1\Pi_u^+$ levels of H_2 [20] and D_2 [32] concerning, however, only the lower levels with $v < 3$.

To provide a coherent and systematic experimental and theoretical account of the absorption spectrum, we carried out systematic calculations of the level energies, the absorption line intensities, and the dissociation widths using MQDT, which is the only “easy” theoretical method for application to the excited levels even if they are predissociated. The theoretical approach used here has been discussed in numerous previous publications [12,33,34] and in particular in our previous papers [13,14,19,26–28]. Briefly, we use quantum defect theory in a simple form by disregarding channel interactions between singly excited and doubly (core) excited Rydberg channels. This means that we assume that the manifold of $^1\Sigma_u^+$ and $^1\Pi_u$ excited states of H_2 represents a single unperturbed np Rydberg series converging to the $X^2\Sigma_g^+$ ground state of the H_2^+ ion.

A. Determination of quantum defects and channel transition moments from quantum-chemical data

The quantum defects have been extracted from highly accurate theoretical clamped-nuclei (Born-Oppenheimer) potential energy curves [29,35] using the familiar one-channel Rydberg equation,

$$U_{np\lambda}(R) = U^+(R) - \frac{1}{2(n - \mu_{np\lambda})^2}, \quad (1)$$

written here in atomic energy units, in order to extract the quantum defects for $^1\Sigma_u^+$ and $^1\Pi_u$ symmetry. $U_{np\lambda}(R)$ is the clamped-nuclei curve for the $np\sigma$ or π Rydberg state, and $U^+(R)$ is the corresponding curve for the ion ground state, $X^2\Sigma_g^+$. The labels $np\lambda$ denote the united-atom Rydberg character of the excited orbitals. The quantum defects $\mu_{np\sigma}$ for the $^1\Sigma_u^+$ symmetry were extracted from the curves corresponding to $n = 3, 4$, and 5 (see Ref. [27] for details) and the quantum defects $\mu_{np\pi}$ for the $^1\Pi_u$ symmetry were extracted from the curves corresponding to $n = 2, 3$, and 4 (see Ref. [26] for the details). Note that the quantum defects determined in this way are functions of the internuclear distance R as well as of the energy because of the dependence on n appearing in Eq. (1). It is the R dependence that mediates the coupling between the electronic and the nuclear degrees of freedom (details can be found in Ref. [26]). As explained in Refs. [26,27], the set of clamped-nuclei quantum defect curves defined by Eq. (1) for the different values of n are converted

into energy-dependent polynomials of the form

$$\mu^{(\lambda,q)}(\varepsilon, R) = \mu^{\lambda,0}(R) + [\varepsilon(R)]\mu^{\lambda,1}(R) + \frac{1}{2}[\varepsilon(R)]^2\mu^{\lambda,2}(R) + \frac{m}{M}\mu^{\lambda,\text{specific}}(R). \quad (2)$$

Here $\varepsilon(R) = U_{np\lambda}(R) - U^+(R)$ is the binding energy of the Rydberg electron for a fixed value of the internuclear distance. The last term (from Refs. [29,36]) has been added and corresponds to the mass polarization correction.

B. Frame transformation

Standard frame-transformation MQDT accounts for nonadiabatic coupling within the Rydberg manifold of states through vibrational-electronic quantum defect matrix elements of the form

$$\mu_{v^+N^+,v'^+N'^+}^{(\lambda,q,N)} = \int_0^{R_c} \chi_{v^+N^+}(R)\mu^{(\lambda,q)}\chi_{v'^+N'^+}(R)dR. \quad (3)$$

The $\mu^{(\lambda,q)}$ are the quantum defect functions of Eq. (2), and $\chi_{v^+N^+}(R)$ are the vibrational eigenfunctions of H_2^+ in the vibrational-rotational level v^+, N^+ , where N^+ is the rotational angular momentum of the electronic ground state of the ion. N refers to the rotational angular momentum of the molecule; in this case, $N = J$, and as the outer electron is in an np state, N^+ and N'^+ may take the values $J - 1$ or $J + 1$ for the interacting $^1\Sigma_u^+$ and $^1\Pi_u^+$ systems. (The value $N^+ = J$ corresponds to the $^1\Pi_u^-$ symmetry [30].) Contrary to the case described previously in Refs. [26,27], where the only nonadiabatic interaction was vibronic and coupled states of the same symmetry, here we must also take into account the rotational coupling mixing the $^1\Sigma_u^+$ and $^1\Pi_u^+$ states and consider the cases in which N'^+ may differ from N^+ .

As detailed in Ref. [26], the integrals in Eq. (3) are converted into a weakly dependent reaction matrix with elements $k_{v^+N^+,v'^+N'^+}^{(N)}(E)$ ($N, N^+ = N \pm 1, N'^+ = N \pm 1$) connecting various Rydberg channels v . At short internuclear distance, the molecule is well described by Hund’s case *b*, and at large distance the electron in the field of the ion corresponds to Hund’s case *d*. The frame transformation has to be taken into account to transform the $\mathbf{k}(E)$ written in the Hund’s case *b* basis set into the $\mathbf{K}(E)$ matrix written in the Hund’s case *d* basis set [28,30].

Standard MQDT procedures [33,34] match the short-range electron wave functions implied by the reaction matrix $\mathbf{K}(E)$ for a given total energy E to asymptotically correctly behaving phase-shifted electron Coulomb waves. It is advantageous to use a sine or cosine formulation rather than the more familiar tangent formulation since in this way poles in the vibrational reaction matrix may be avoided [33]. The boundary condition then reads

$$\det[\cos \beta(E)S + \sin \beta(E)C] = 0, \quad (4)$$

where $\mathbf{K} = \mathbf{S}\mathbf{C}^{-1}$ and $\beta(E)$ is an asymptotic phase vector whose components $\beta_{v^+}(E)$ take different values depending on whether a given N^+ Rydberg channel is closed ($E < E_{v^+}$) or open ($E > E_{v^+}$). For closed channels, $\beta_{v^+}(E) = \pi\nu_{v^+}$, with $\nu_{v^+} = (2^{-1/2})[(E_{v^+} - E)]^{-1/2}$ the effective principal quantum number corresponding to that channel. Here we considered

only the closed channel, thus we disregarded the ionization process. For the D state, the autoionization is extremely weak and could be neglected [12].

C. Bound levels and discrete line intensities

Once an energy E has been found such that Eq. (4) is satisfied, the level energy, taken relative to the ionization potential and in wave-number units, becomes

$$(E - E_{v^+N^+})/hc = -\frac{\text{Ry}_{\text{H}_2}}{(v^+N^+)^2}, \quad (5)$$

where Ry_{H_2} is the mass-corrected Rydberg constant and E is the level energy in joules. [The use of the mass-corrected Rydberg constant instead of the Rydberg constant is equivalent to including the term $-(m/2M)\nabla_1^2$ of the molecular Hamiltonian, which, in the standard approach, is a part of the adiabatic correction.]

The required energy-normalized dipole transition moments are extracted from the available *ab initio* dipole transition moments from Refs. [29,35], in a fashion similar to what has just been described for the quantum defects. These are used to calculate energy-dependent channel transition moment coefficients $d^{(\lambda,q)}(\varepsilon, R)$ analogous to the quantum defect coefficients $\mu^{(\lambda,q)}(\varepsilon, R)$ of Eq. (2). Vibronic channel dipole transition matrix elements $d_{v^+N^+,v''N''}^{(\lambda,q,N)}$ are evaluated from an equation similar to Eq. (3), where d replaces μ and $\chi_{v''N''}(R)$ replaces $\chi_{v^+N^+}(R)$. The change from Hund's case b to Hund's case d changes the \mathbf{d} matrix into a \mathbf{D} one mixing the v^+ , N^+ and v^+ , N^+ channels.

The effective transition moment to a bound Rydberg level n is given by the following superposition of channel amplitudes:

$$D_n^\lambda = \frac{1}{\mathcal{N}} \sum_k D_{k,k''}^\lambda(E_n) B_k(E_n), \quad (6)$$

where B_k are the channel mixing coefficients obtained by solving Eq. (4) and k stands for the combination of ionization channels v^+, N^+ and v^+, N^+ for a $\lambda = \sigma$ or π state; k'' stands for $v'' = 0, N''$; \mathcal{N} is the overall normalization factor of the bound state wave function.

The rotational couplings mix the $\lambda = \sigma$ and $\lambda = \pi$ states modifying the intensities of the R and P lines to the considered n level of total angular momentum quantum number N according to

$$A(R) = \frac{4}{3} \frac{mc^2}{\hbar} \alpha^5 \left[\sqrt{\frac{N}{2N+1}} \frac{D_n^\sigma}{a_0} - \sqrt{\frac{N+1}{2N+1}} \frac{D_n^\pi}{a_0} \right]^2 \times \left(\frac{E_n - E_{vN}}{2hc \text{Ry}} \right)^3 \quad (7)$$

for an $R(N - 1)$ line [28,37,38] and

$$A(P) = \frac{4}{3} \frac{mc^2}{\hbar} \alpha^5 \left[\sqrt{\frac{N+1}{2N+1}} \frac{D_n^\sigma}{a_0} + \sqrt{\frac{N}{2N+1}} \frac{D_n^\pi}{a_0} \right]^2 \times \left(\frac{E_n - E_{v''N''}}{2hc \text{Ry}} \right)^3 \quad (8)$$

for a $P(N + 1)$ line. Here α is the fine-structure constant. The transition energy is in joules and the transition moment

in meters. The ratios in the large parentheses and in the large square brackets correspond, respectively, to the transition energy and to the dipole moment in atomic units (see Ref. [28] for more details).

D. Dissociation continuum

The inclusion of dissociation channels into the MQDT framework has been described previously [11,12,25]. The approach described in those papers was simplified here since we are able to neglect the interference between ionization and dissociation processes. We proceed as follows. Our treatment of dissociation is based on the realization that the dissociating state in the present problem is the $3p\sigma B'$ state and, as such, is simultaneously a low member of the $p\sigma$ ionization channel (which we are considering here) and therefore plays a double role. This implies that the nonadiabatic coupling leading to vibrational autoionization of the $np\sigma$ manifold above threshold *is the same* as that causing predissociation by the $3p\sigma B'$ state. Therefore, the vibronic quantum defect matrix elements $\mu_{v^+N^+,v''N''}^{(\lambda,q,N)}(E)$ of Eq. (3) contain *all* the information required to evaluate the predissociation widths in addition to the autoionization widths. We exploit this circumstance by choosing specifically adapted vibrational basis sets for solving Eq. (4). Considering a specific value of the total energy E , we evaluate the vibrational wave functions χ_{v^+} and energies E_{v^+} by using a "large" vibrational basis, chosen such that it corresponds to electronically bound Rydberg channels only, whereas all the open channels ($E_{v^+} < E$) are omitted. A *common* boundary condition $b = -\chi'/\chi$ is imposed on all χ_{v^+} at $R = R_c$. With a large basis, the bound ion target vibrational levels [$E_{v^+} < U^+(R_c)$] remain at their correct energies, but the level spectrum $E_{v''}$ now extends beyond the bound range into the H^+_2 vibrational continuum where the energies depend on the particular boundary condition b used.

Similarly, solving Eq. (4) yields the Rydberg levels corresponding to $n \geq 3$ with $v < v^+_{\text{last bound}}$ near their correct energies, but in addition, a set of fictitious Rydberg levels with $n = 2, v^+ > v^+_{\text{last bound}}$ is obtained, which represents the *discretized* $2p\pi C$ or $2p\sigma B$ state vibrational continuum, as well as another one with an $n = 3, v^+ > v^+_{\text{last bound}}$ which represents the *discretized* $3p\sigma B'$ state (see also Ref. [12]). When the boundary condition b at $R = R_c$ is varied, these levels may be tuned through the position of a bound Rydberg level with $n = 3, v < v^+_{\text{last bound}}$. Nonadiabatic interaction leads to an *avoided crossing* characterized by a closest approach $2V$. From this, the predissociation width Γ may be extracted using Fermi's "Golden Rule,"

$$\Gamma_d = 2\pi \frac{V^2}{\Delta E}. \quad (9)$$

Here ΔE^{-1} is the density of levels of the discretized continuum. This procedure had been used previously [14] to calculate the predissociation widths of the $3p\pi D^1\Pi_u^-$ levels which are very small. We extended its application to a case in which the predissociation widths are large. The results obtained here for the $J = 2 3p\pi D^1\Pi_u^+$ levels are similar to the values calculated previously in a more sophisticated way [11].

The coupling to the $3p\sigma B'$ continuum is so strong for the $3p\pi D^1\Pi_u^+$ levels that the position of the bound Rydberg level with $n = 3$, $v < v_{\text{last bound}}^+$ varies by an amount comparable to its width, which is far too large to be acceptable. Under the same conditions as described above, we fixed the b parameter and varied the R_c value; the position of the resonance varies according to the bypass of the quasicontinuum levels around a mean value, which is the desired result. The intensity of the absorption line is calculated from an average in the same way. The results are independent of the fixed value of b (from 0 to 10^6); they correspond to the D level positions lying at equal distances from both nearby quasidecrete B' levels. The variations of R_c are just a technical way of varying the positions of the interacting quasidecrete levels.

E. D₂ calculations

The same computational method was used for the D₂ molecule, just changing the value of the reduced mass and the value of the mass-corrected Rydberg constant in Eq. (5). The mass dependence of the adiabatic corrections to the potential curves was hereby implicitly taken into account.

F. Numerical details

The vibration-rotation wave functions χ_{v+N^+} were evaluated in the adiabatic approximation using the ion ground-state potential energy curve of Wind [39] and the adiabatic correction terms of Bishop and Wetmore [40]. The corresponding ion levels E_{v+N^+} are those of Wolniewicz and Orlikowski [41], calculated by including the nonadiabatic and relativistic interactions in addition to the adiabatic corrections. The ground-state vibrational wave function $\chi_{v''N''}(R)$ was evaluated by using the potential energy curve of Wolniewicz [37] (with adiabatic corrections).

The upper limit R_c of the integral over dR in Eq. (3) was varied between $R_c \approx 7$ and ≈ 15 a.u. and the vibrational basis typically contained between 20 and 45 vibrational functions (i.e., between 40 and 90 channels).

III. EXPERIMENT

The experimental data of Refs. [21,22] have been completed by additional data extracted from the BESSY spectra concerning the line intensities and the dissociation widths of H₂. The experimental setup at BESSY has been described in detail in previous publications [14,42–45]. The VUV radiation from the undulator beamline U125/2-10m-NIM of BESSY II was dispersed by a 10-m normal-incidence monochromator equipped with a 4800 lines/mm grating giving a spectral resolution of 0.0010 nm in first order [46] (this value represents the convolution of the apparatus function with the Doppler width at room temperature). The uncertainty of the energies of the measured spectra is at present typically ± 1.0 to ± 1.5 cm⁻¹. The intensity of the absorption spectrum, recorded at high spectral resolution, has been calibrated directly, based on the known gas pressure and the absorption path length. Photoionization and photodissociation excitation spectra were recorded

simultaneously. The absolute calibration of these spectra has been described in detail previously (see Refs. [14,42–45]).

The energy values of the D levels for H₂ and D₂, obtained with the Fourier-transform spectrometer of SOLEIL and the BESSY experiment have been presented and compared in Refs. [21,22]. From the dissociation spectrum obtained at BESSY, it was also possible to extract the widths and the intensities of the lines. These lines were fitted by a convolution of a Fano profile with a Gaussian corresponding to the apparatus function, taking into account the Doppler width [14]. The absolute intensities and the widths of the $3p\pi D^1\Pi_u^+$, v , $J - Xv'' = 0$, J'' lines have been determined systematically by means of the dissociation excitation spectrum through such a fit, giving a set of data for H₂. The linewidths of Ref. [21] were from the SOLEIL experiment. For D₂, the BESSY data and the SOLEIL ones have been combined and gathered in Ref. [22]. The present measurements add few complements. The H₂ $R(2)$ line data were not reported before.

IV. RESULTS

A. Level energies and Λ doubling

1. H₂ molecule

The energies of the $3p\pi D^1\Pi_u^+$ $J = 1$ and 2 , $v = 0$ – 15 , levels of H₂ have been determined with an uncertainty of 0.3 cm⁻¹ from the FT spectrum; for $v = 16$ and 17 , the energy values are from the BESSY experiment with an uncertainty of 1 cm⁻¹ (all of them are in Ref. [21]). We compared these values with the calculated ones. The discrepancy [$E(\text{obs}) - E(\text{calc})$] is lower than 1 cm⁻¹, much smaller than the dissociation widths, except for the last vibrational quantum number. The present calculations are clearly more precise than those of Gao *et al.* [11], who used only the quantum defects deduced from one $\Pi(3p\pi D)$ state and one $\Sigma(4p\sigma)$ state, consequently without any energy dependence, leading to an insufficient description of the nonadiabatic couplings with the other levels. The present results are comparable to those of the full treatment of Ref. [12], although our approach is a simplified one. The MQDT values obtained for the $v = 0$ – 2 levels, which lie below the dissociation threshold, can be compared with the values obtained by the CE approach [20]. As has already been observed [19] for the 2 and $3p\pi^1\Pi_u^-$ levels, the MQDT approach gives more precise results for levels with $n \geq 3$. The results are gathered for comparison in Table I.

The calculations are precise enough to determine the Λ doubling of the $J = 1$ and 2 D levels of H₂. The experimental data for the $3p\pi D^1\Pi_u^-$ are from Ref. [21] and the MQDT calculated values are from Ref. [14]. The results are gathered in Fig. 1 with the calculated values from Ref. [20]. Obviously, both calculations reproduce the erratic behavior of the levels located below the dissociation threshold which are interacting with the bound B' levels. The MQDT is also able to reproduce the accidental situation of the $v = 7$ levels; the $J = 1$, $v = 7$, $3p\pi D^1\Pi_u^+$ level lies very near the $J = 1$, $v = 5$, $4p\sigma B''$ level so that these levels interact through the $3p\sigma$ continuum to which they are both coupled. This local perturbation leads to an unexpected negative value of the Λ doubling. The $J = 2$ levels of D and B'' are not so close and the perturbative effect is weaker. Globally, the Λ doubling decreases to zero at the

TABLE I. Calculated and measured values for the R lines ($0-v$) of H_2 . In column 3, obs.-calc. is the deviation: observed-calculated values (in cm^{-1}). The observed transition energies are from Ref. [21] for $J = 1$ and 2 and from Ref. [3] for $J = 3$ with $v < 6$. The bold values correspond to experimental data of the present work. Calculated and measured A Einstein coefficients for the R lines, present work. Calculated and measured dissociation widths (in cm^{-1}): present work.

v	$J = 1$						$J = 2$					
	E_{calc}	obs.-calc.	A_{calc} ($10^6 s^{-1}$)	A_{meas}	Γ_{calc}	Γ_{meas}	E_{calc}	obs.-calc.	A_{calc} ($10^6 s^{-1}$)	A_{meas}	Γ_{calc}	Γ_{meas}
0	112 935.40	-0.15	21.86				112 940.93	0.27	19.77			
1	115 155.87	-0.07	42.39				115 150.85	0.29	37.93			
2	117 251.67	-0.03	43.21				117 244.58	0.24	35.47			
3	119 218.82	-0.83	38.35		4.19		119 203.86	-0.26	33.40			
4	121 062.87	0.18	31.17		4.13		121 042.09	0.39	26.55			
5	122 787.68	0.26	22.92		4.01		122 761.15	-0.29	18.78			
6	124 394.01	-0.26	15.10	21 ± 3	4.44	4.7 ± 0.3	124 360.68	-0.98	12.36	12 ± 2	14	12.2 ± 0.5
7	125 877.16	-0.13	25.88	26 ± 4	3.77	- \pm -	125 840.71	0.64	15.57	14 ± 2	13.7	9.6 ± 0.5
8	127 248.00	-1.16	6.91	6.6 ± 1.0	4.15	4.4 ± 0.3	127 203.09	-1.94	7.41	6.7 ± 1.0	13.75	12 ± 0.5
9	128 496.80	-0.26	5.45	5.6 ± 0.8	3.27	3.7 ± 0.3	128 444.37	0.57	5.21	4.2 ± 0.6	12.24	9.9 ± 0.5
10	129 622.17	-0.74	3.73	3.3 ± 0.5	3.35	3.1 ± 0.3	129 563.87	-0.07	3.45	2.8 ± 0.4	12.29	10 ± 0.5
11	130 618.27	0.25	3.50	3.3 ± 0.5	2.97	2.9 ± 0.3	130 553.59	0.56	3.02	2.4 ± 0.4	11.7	8 ± 0.5
12	131 484.71	-0.21	1.91	2.7 ± 0.4	2.76	2.2 ± 0.3	131 414.89	-0.89	1.84	1.5 ± 0.2		7 ± 0.5
13	132 212.15	0.18	1.02	1.2 ± 0.2	2.38	2.2 ± 0.3	132 134.91	-0.44	0.86	0.8 ± 0.1		5.7 ± 0.5
14	132 791.62	0.75	0.93	0.99 ± 0.15	2.32	1.5 ± 0.3	132 706.67	0.22	0.80	0.58 ± 0.09		3.7 ± 0.5
15	133 219.52	-0.18	0.58	0.61 ± 0.09	0.80	0.8 ± 0.3	133 125.46	-0.50	0.55	0.50 ± 0.07		3.3 ± 0.5
16	133 485.00	-0.41	0.20	0.26 ± 0.04		0.8 ± 0.3	133 381.96	-0.85	0.16	0.18 ± 0.03		1.8 ± 0.5
17	133 586.00	1.77	0.05	0.11 ± 0.02		0.5 ± 0.3	133 481.25	-8.63	0.07	0.022 ± 0.003		1.5 ± 0.5

$J = 3$					
v	E_{calc}	obs.-calc.	A_{calc} ($10^6 s^{-1}$)	A_{meas}	Γ_{meas}
0	112 889.22	0.81	17.8		
1	115 083.06	0.80	35.8		
2	117 171.93	0.41	29.9		
3	119 119.14	-1.53	27.2		
4	120 952.43	-1.15	20.0		
5	122 655.86	-2.25	15.8		
6	124 264.35	2.21	7.80	10.0 ± 2.5	24 ± 2
7	125 726.71	3.74	6.64	5.7 ± 1.4	17 ± 2
8	127 082.04	6.51	5.14		
9	128 305.77	4.04	7.05	6.2 ± 1.6	24 ± 2
10	129 418.87	-3.11	4.16	4.5 ± 1.1	22 ± 2
11	130 399.84	3.75	4.12	2.9 ± 0.7	20 ± 2
12	131 246.83	6.26	2.58	1.5 ± 0.4	13 ± 2
13	131 965.62	1.15	0.31		
14	132 521.75	3.15	1.11	1.2 ± 0.3	9.5 ± 1
15	132 923.04		0.58		
	133 166.11	-1.49	0.13	0.17 ± 0.04	2.6 ± 0.4

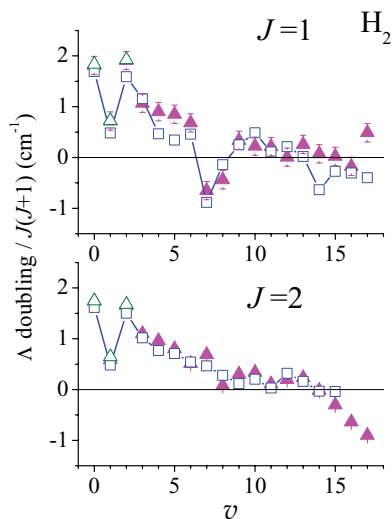


FIG. 1. (Color online) The Λ -doubling values [divided by the factor $J(J+1)$] for the $J = 1$ and 2 H_2 levels in the $3p\pi D^1\Pi_u$ state plotted against vibrational quantum number v . A plus sign indicates that $^1\Pi_u^+$ or e levels are higher than $^1\Pi_u^-$ or f levels. Filled triangles (magenta): experimental data from Ref. [21]. Open squares (blue): present MQDT calculations. Open triangles (green): CE calculations [47].

dissociation limit: the coupling between the $3p\pi$ state and the $3p\sigma$ continuum occurs at short internuclear distance and, as the vibrational energy increases, the time spent by the system at short distances decreases.

For the $J = 3$ levels of the $3p\pi D^1\Pi_u^+$ state of H_2 , the calculations reproduce the experimental energy values [3,4] within the experimental uncertainty ($<1 \text{ cm}^{-1}$) for the levels with $v < 3$. For the levels with $v \geq 3$, the predissociation width is very large ($>20 \text{ cm}^{-1}$ for the levels with $v = 3-10$) and the differences [$E(\text{obs}) - E(\text{calc})$] are within the predissociation widths. We were able to determine the energies of eight of the $R(2)$ lines with an uncertainty of the order of 2 cm^{-1} through a Fano fit. The agreement with the calculated values is greatly improved (see Fig. 2, lower part) and remains within the experimental error except for the $v = 12$ value, for which the discrepancy is twice the experimental uncertainty.

2. D_2 molecule

The vibrational series of the D state of D_2 extends from $v = 0$ to 23. The experimental energies of the $3p\pi D^1\Pi_u^+$ levels $J = 1$ and 2 , $v = 0-16$, and $J = 3$, $v = 0-7$, of D_2 are known with an uncertainty of $0.06-0.4 \text{ cm}^{-1}$ from the FT spectrum; all the other values in Ref. [19], including the $J = 4$ ones, are from the BESSY experiment with an uncertainty of 1 cm^{-1} . The difference between these experimental values and the MQDT calculated values is below 1 cm^{-1} , clearly smaller than the dissociation widths (see Fig. 3); they are found to increase with J . Since the dissociation widths increase with J , the process used to determine the energies experimentally becomes less and less precise as J increases. The energies of the $v = 0-4$ $3p\pi D^1\Pi_u^+$ unpredissociated levels have been

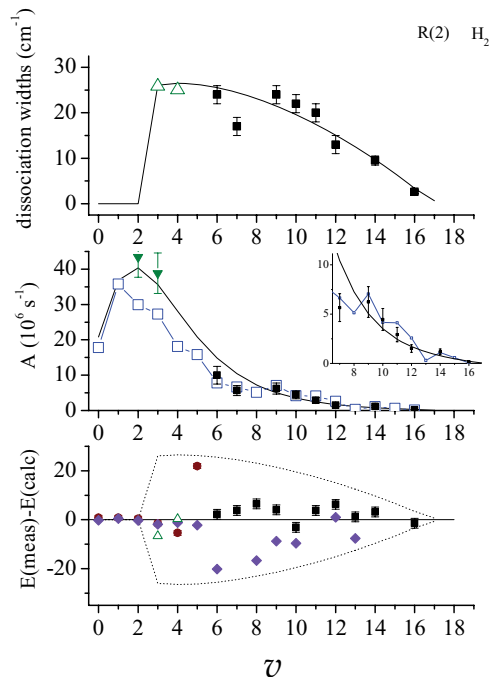


FIG. 2. (Color online) Lower trace: residual obs.-calc. (in cm^{-1}) for the $J = 3 D^1\Pi_u^+$ levels of H_2 , plotted as functions of the vibrational quantum number v . The calculated values are the present MQDT data. Filled squares (black): present experimental data. Filled diamonds (violet): experimental data from Ref. [3]. Filled circles (brown): experimental data from Ref. [4]. Open triangles (green): experimental data from Ref. [3] and CE calculations [24]. Dotted line: $+/-$ the dissociation widths calculated in Ref. [21]. Middle trace: the intensities of the $R(2) D-X (v=0)$ lines vs v . Filled squares (black): present experimental data. Open squares (blue): present MQDT calculations. Filled down triangles (green): experimental data from Ref. [8]. Full line: adiabatic calculations. Inset: enlarged section corresponding to large v . Upper trace: the dissociation widths of the $J = 3 D^1\Pi_u^+$ levels. Filled squares (black): present experimental data. Open triangles (green): calculated values from Ref. [24]. Full line: the dissociation width calculated in Ref. [21].

calculated using coupled equations by Roudjane *et al.* [32]. The present calculations are clearly more precise than the CE calculations, as was also the case for the calculations of the $3p\pi D^1\Pi_u^-$ levels [19].

The calculated level energies (and the calculated line intensities) allow a systematic study of the spectrum and the assignment of new lines: $R(2)$ of the $D-X (23,0)$ band, $R(3)$ of the $(20,0)$, $(22,0)$, and $(23,0)$ bands, and $R(4)$ of the $(19$ to $21,0)$ bands. These new lines were drawn with error bars in Fig. 3. One misprint in Ref. [22] could also be corrected, namely $R(2)$ of the $(14-0)$ band as a wrong value for the $R(2)$ $(22,0)$ band (see Table II).

Using the experimental data from Ref. [22] for the $3p\pi D^1\Pi_u^-$ levels and the MQDT calculated values from Refs. [19,26], the Λ doubling was deduced and compared with the experimental values of Ref. [22]. The results are displayed in Fig. 4. They follow partly the $J(J+1)$ scale rule, indicating that the simple model of a rotational coupling between the $3p\pi D^1\Pi_u^+$ and the $3p\sigma B^1\Sigma_u^+$ states is not

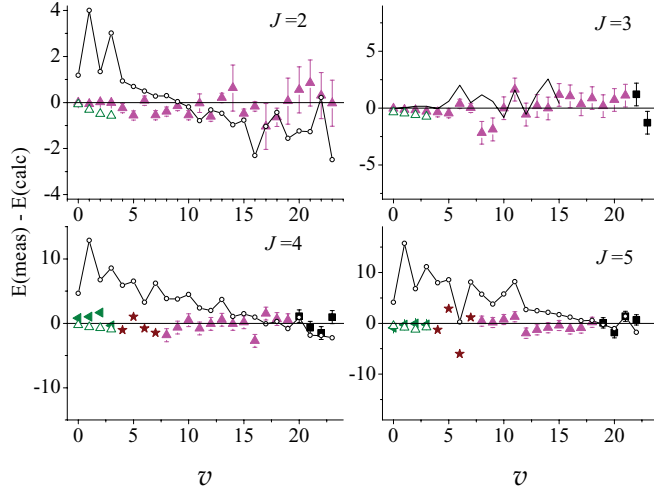


FIG. 3. (Color online) Residual obs.-calc. (in cm^{-1}) for the level energies of the $3p\pi D^1\Pi_u^+$ state of D_2 . Filled triangles (magenta): experimental values from Ref. [22] and present MQDT data. Filled squares (black): present experimental data and present calculated values. Open triangles (green): experimental values from Ref. [22] and CE calculations [32]. Filled stars (brown): experimental data from Ref. [3] and present MQDT data. Filled left triangles (green): experimental and CE calculated values from Ref. [32]. Full line (black): experimental and adiabatic calculations from [22].

quite sufficient to reproduce the experimental results, even if it is obvious that no strong local perturbations affect the levels.

TABLE II. Calculated and measured values for the $J D$ levels of D_2 . obs.-calc. is the deviation: observed-calculated values (in cm^{-1}). The observed R transition energies are from Ref. [22] for $J = 1-5$ except for the values $J = 4$ and 5 and $v = 0-3$, which are from Ref. [32], and $J = 4$ and 5 and $v = 4-7$, which are from Ref. [3] for $J = 3$ with $v < 6$. The bold values correspond to the experimental data of the present work.

v	$J = 1$		$J = 2$		$J = 3$		$J = 4$		$J = 5$	
	E_{calc}	obs.-calc.	E_{calc}	obs.-calc.	E_{calc}	obs.-calc.	E_{calc}	obs.-calc.	E_{calc}	obs.-calc.
0	113 223.03	-0.06	113223.69	0.00	113 194.68	-0.04	113 135.83	0.80	113047.20	-0.90
1	114 825.17	-0.06	114825.54	-0.06	114 795.68	-0.13	114 735.08	1.03	114644.00	-0.31
2	116 359.59	-0.03	116356.17	0.01	116 321.21	-0.18	116 254.16	1.65	116155.32	-0.05
3	117 831.50	-0.03	117827.07	-0.01	117 790.16	-0.29	117 719.84	-0.34	117616.43	-0.23
4	119 238.70	0.15	119231.69	-0.24	119 190.15	-0.36	119 116.99	-1.04	119008.36	-1.30
5	120 585.10	0.28	120576.33	-0.56	120 531.96	-0.45	120 453.03	1.02	120337.18	2.88
6	121 871.31	-0.24	121859.05	0.08	121 811.69	0.39	121 728.24	-0.79	121609.48	-6.02
7	123 096.50	-0.01	123083.07	-0.55	123 032.20	0.03	122 948.41	-1.46	122821.80	1.16
8	124 262.81	-0.59	124246.64	-0.39	124 194.67	-2.17	124 103.35	-1.85	123972.16	0.44
9	125 369.01	-0.53	125350.49	-0.15	125 295.87	-1.87	125 199.67	-0.67	125063.13	0.17
10	126 415.01	0.50	126395.68	-0.55	126 336.01	-0.01	126 237.41	0.49	126097.86	0.74
11	127 402.26	0.89	127380.61	-0.03	127 316.76	1.64	127 215.20	-0.80	127073.41	1.29
12	128 330.68	0.02	128307.08	-0.61	128 241.26	-0.56	128 132.69	-0.09	127984.74	-1.94
13	129 197.83	-0.17	129170.94	0.20	129 102.41	0.19	128 991.56	0.54	128836.59	-1.29
14	130 003.02	-0.14	129972.37	0.63	129 901.79	-0.02	129 785.50	-0.10	129626.58	-0.88
15	130 744.70	0.48	130714.76	-0.48	130 637.63	1.17	130 518.34	0.16	130353.03	-0.43
16	131 423.60	-0.48	131388.47	-0.17	131 310.05	1.05	131 188.42	-2.72	131015.30	-1.09
17	132 034.29	-0.16	131999.18	-1.04	131 915.46	0.34	131 783.80	1.50	131609.31	-0.91
18	132 576.40	-0.10	132538.17	-0.64	132 450.72	0.88	132 316.25	0.65	132133.39	0.21
19	133 046.06	0.64	133005.70	0.06	132 916.02	0.18	132 774.53	0.47	132585.46	0.09
20	133 442.51	0.39	133399.07	0.55	133 304.78	0.73	1331 60.03	1.09	132964.12	-1.84
21	133 761.97	1.03	133715.59	0.85	133 616.69	1.11	133 465.71	-0.69	133262.66	1.37
22	134 001.66	0.94	133954.99	0.30	133 848.38	1.21	133 692.53	-1.52	133478.24	0.67
23	134 158.35	0.65	134105.22	1.48	133 995.90	-1.28	133 831.37	0.96		

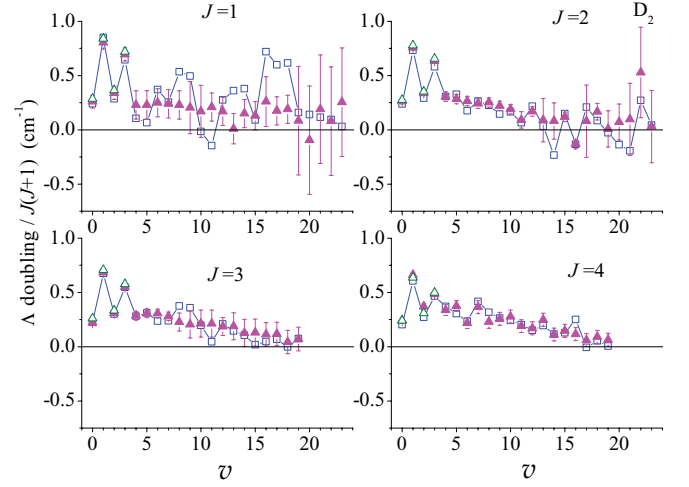


FIG. 4. (Color online) Same as 1 for D_2 . The experimental data are from Ref. [22]. The CE calculations are from Ref. [32].

B. Line intensities

We have extracted Einstein A coefficients corresponding to each observed line using the relation

$$\int \sigma d\lambda = \frac{\lambda^4}{8\pi c} A_{v',v'',N',N''} \frac{2N' + 1}{2N'' + 1} n_{N''} \quad (10)$$

with $N' = N'' + 1$ for an $R(N'')$ line and $N' = N'' - 1$ for a $P(N'')$ line. Here λ is the wavelength, $n_{N''}$ is the

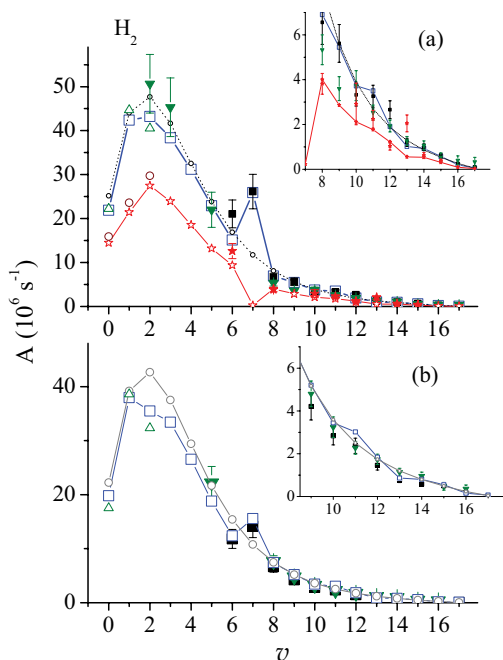


FIG. 5. (Color online) H_2 line intensities vs v . Upper trace: $R(0)$ and $P(2)$ lines. Lower trace: $R(1)$ lines. Filled squares (black): present experimental data for R lines. Filled stars (red): present experimental data for P lines. Open squares (blue): present calculated values for R lines; open stars (red): present calculated values for P lines. Filled down triangles (green): data from Ref. [8]. Open triangle (green) and open triangles (brown): CE calculated values for R and P lines, respectively, from Ref. [47]. Open circles connected by full lines (gray): adiabatic values. Inset: enlarged sections corresponding to large v .

fraction of molecules in the rotational state N'' , and σ is the measured absorption cross section which is integrated over the Beutler-Fano profile of a given line. As the dissociation yield for these lines is practically 100%, the integration was done in the dissociation spectrum, which is less noisy.

1. H_2 molecule

We were able to measure the absolute intensities of the $R(N'')$ ($N'' = 0-2$) and $P(2)$ lines of H_2 for the vibrational progression from $v = 6$ to 16, except for a few cases in which the lines were superposed to other lines. The MQDT calculated intensity values are displayed in Fig. 5 with the experimental data. The intensities calculated in the adiabatic approximation are displayed for comparison. Globally, the differences between the nonadiabatic and the adiabatic values are quite small. This result is quite surprising because in the case of the $3p\pi D^1\Pi_u^-$ system, it was shown that nonadiabatic couplings, while only weakly affecting the level energies, have a major effect on the intensities of the $Q(N)$ absorption lines [26]. The $3p\pi D^1\Pi_u^+$ state is coupled mainly to the $3p\sigma B'^1\Sigma_u^+$ state, which is a continuum at energies higher than the $D v = 2$ levels. A coupling with a continuum changes the shape of the line but not its energy-integrated intensity value. For one level, namely $v = 7$, $J = 1$, the local perturbation with the $4p\sigma B'' v = 5$, $J = 1$ level is strong enough to be visible on the Λ doubling (and so on the

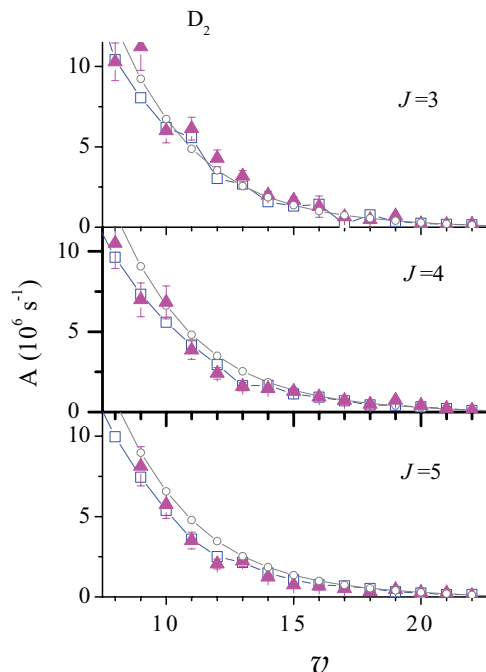


FIG. 6. (Color online) Same as Fig. 5 for D_2 $R(J)$ lines; the experimental data are from Ref. [22].

energy) and on the intensities of the lines; we can see clearly the opposite variations of the intensities of the $R(0)$ and $P(2)$ lines. The calculated values reproduce the observed intensities within the error bars.

For the levels $v = 0-2$, the values calculated using a CE approach [47] (in order to improve the agreement with experimental energy values, these calculations were not completely *ab initio*) are also displayed in Fig. 5, showing a good agreement with the MQDT values. Earlier measurements of the band transitions [8] scaled by the adiabatic Hönl-London factors are also displayed in Fig. 5 for comparison. The intensities of the $R(2)$ lines are displayed in Fig. 2; as expected, the nonadiabatic couplings are more efficient and could be put into evidence experimentally. The MQDT calculations reproduce the experimental data.

2. D_2 molecule

The MQDT calculated intensity values of the $R(J)$ lines for $J = 3-5$ are displayed with the experimental and the adiabatic values in Fig. 6. For $J = 1$ and 2, the difference between the adiabatic and nonadiabatic values is within the error bars. For $J = 3-5$, the effects of the nonadiabatic couplings begin to be visible at the experimental intensities and could be accounted for by the MQDT calculations.

For the lower levels with $v = 0-3$, the MQDT values agree with the *ab initio* CE calculated values of Ref. [32] within 5% in all the cases except for $v = 1$, where the disagreement rises to 10% with a particular case of 15%: the $R(1)$ (1,0) line. For this band, the nonadiabatic decrease of the intensity (which increases with J , as expected) amounts to 32% for the CE calculation and to 23% for the MQDT one. However, for the $R(1)$ (1,0) line, we have no experimental data to compare with.

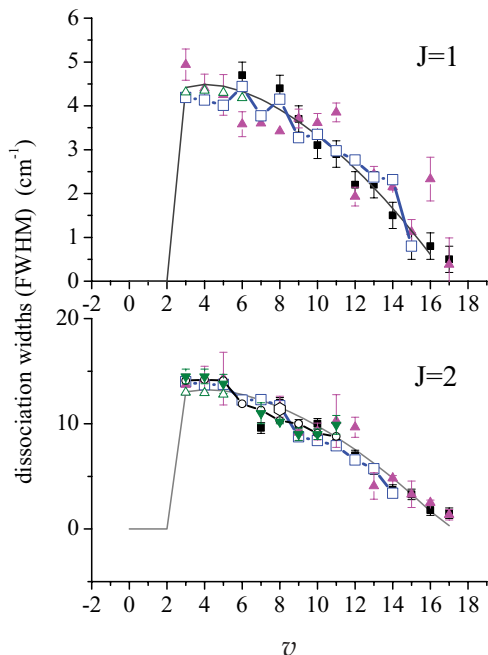


FIG. 7. (Color online) Dissociation widths (FWHM) in cm^{-1} vs v for the $J = 1$ (upper trace) and $J = 2$ (lower trace) $\text{H}_2 D^1\Pi_u^+$ levels. Filled triangles (magenta): experimental data from Ref. [21]. Filled squares (black): present experimental data. Filled triangles (green): experimental data from Ref. [6]. Open squares (blue) connected by full lines: present calculated values. Open circles connected by full lines (black): MQDT calculated values from Ref. [13]. Open triangles (green): CE calculations from Ref. [24]. Gray line: calculated value from Ref. [21] (see text).

C. Dissociation widths

1. H_2 molecule

Under the conditions of the recording of the spectrum, the apparatus function (taking into account the Doppler widths of the lines) is $1.2\text{--}1.5 \text{ cm}^{-1}$ with a Gaussian shape; this apparatus function was studied on the $D Q$ lines for which the natural width is known to be around $2 \times 10^{-3} \text{ cm}^{-1}$ and is therefore completely negligible [18]. Through a fit of the line profiles with a convolution of this Gaussian with a Fano profile, we have been able to determine the experimental widths of the excited levels with $J = 1\text{--}3$. This new set of values is compared with previously measured values (see Fig. 7). The scatter of the data is an indication of the uncertainty which is probably systematically underestimated.

In Ref. [21], the dissociation widths were calculated with a perturbative approach as initiated by Julienne [9] and using the up-to-date coupling functions and adiabatic potentials of Ref. [20]. These values agree globally with the experimental data.

We calculated the dissociation widths using MQDT as described in Ref. [14]. The $J = 1$ level widths, calculated in this way, agree very well with the experimental data. They show variations due to the nonadiabatic couplings with the other bound states even if this effect is small (there are only little differences between the two calculations). The present MQDT results for the $J = 2$ level widths reproduce the experimental data and are very near the previously calculated

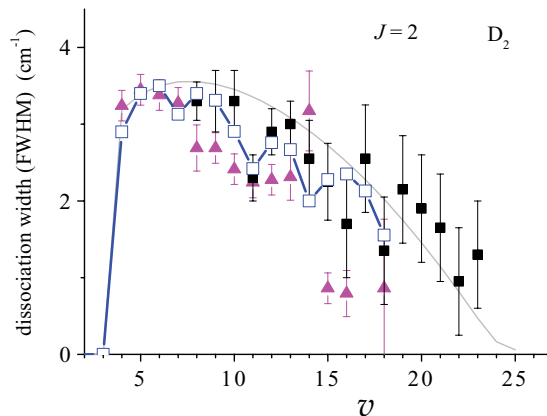


FIG. 8. (Color online) Same as Fig. 7 for the $J = 2 D^1\Pi_u^+$ levels of D_2 .

ones [11,12] (see Fig. 7); however, this simple approach of the dissociation calculations by MQDT is not really adequate for these very broad lines, as they were found to be very sensitive to the calculation conditions, and so these results are less reliable than those for $J = 1$, especially for $v > 9$.

2. D_2 molecule

The predissociation widths of the $J = 1\text{--}5, v, 3p\pi D^1\Pi_u^+$ levels of D_2 have been reported in Ref. [22]. The widths of the $J = 1$ levels are quite small, i.e., of the order of 1 cm^{-1} or less. Their relative uncertainty is too high to show any nonadiabatic effect different from the $3p\pi\text{--}3p\sigma$ coupling. For the $J = 3\text{--}5$ levels with $v \geq 8$, the perturbative calculations reproduce very well the observed data.

For the $J = 2$ levels, the quality of the data is high enough to put into evidence the effect of the nonadiabatic couplings different from the $3p\pi\text{--}3p\sigma$ one. The deviations of the experimental values from the values calculated by the perturbative approach are well reproduced by the MQDT calculations (see Fig. 8).

Globally, the dissociation widths are proportional to the squared coupling matrix element between the $3p\pi D^1\Pi_u^+$ levels and the $3p\sigma B^1\Sigma_u^+$ continuum. This Coriolis matrix element is proportional to $1/\mu$, μ being the reduced mass, so that the dissociation widths of H_2 and D_2 are expected to scale in the isotopic ratio of 4:1, as is roughly observed.

V. CONCLUSION

We presented nonadiabatic, *ab initio*, systematic calculations of the $3p\pi D^1\Pi_u^+$ level energies and absorption line intensities for H_2 and D_2 even for those levels that are strongly predissociated. The energies of the resonances are well reproduced, with the difference $E(\text{obs}) - E(\text{calc})$ being smaller than 1 cm^{-1} in most cases, generally much smaller than the dissociation widths of the levels. These calculations were performed using a simple version of MQDT, i.e., under the assumption that up to moderate R values, the excited electronic states are correctly described as $n\pi$ electrons interacting with the vibrating and rotating ground-state H_2^+ ion. The nf configuration of the outer electron and the excited states of the

ion have been neglected. Even in this simple form, the MQDT approach is able to reproduce very well the experimental level energies ($\ll 1 \text{ cm}^{-1}$) for the discrete levels ($v < 3$ for H_2 or $v < 4$ for D_2). For the dissociated levels, where no CE energies (nor intensities) had been calculated so far, the MQDT calculations reproduce very well the experimental level energies within 1 cm^{-1} in most cases, i.e., the deviations are much smaller than the dissociation widths.

The precision of our calculations allows us to determine the Λ doublings. The calculations reproduce correctly the experimental data, even when they are negative due to a local strong perturbation.

The intensities of the absorption lines have been calculated and compared with measured absolute values (new data set or previously published data) and were found to agree within the experimental error bars. In this paper, seven additional lines could be assigned, and several experimental data, such as level energies, line intensities, and dissociation widths, were revisited and corrected. For the dissociation widths, the importance of local nonadiabatic perturbations is small (affecting the widths by percents only) compared to the main $3p\pi$ - $3p\sigma$ coupling, as could be concluded from the comparison between the MQDT and the perturbative calculated values.

In the framework of an effort to provide a coherent and systematic experimental and theoretical account of the absorption spectrum of diatomic hydrogen and its isotopomers up to the $H(1s) + H(n = 4)$ dissociation limit, we have so far described the $^1\Pi_u^-$ levels subject to only weak vibronic couplings [26], the $J = 0$ $^1\Sigma_u^+$ levels affected by strong vibronic couplings [27], and the $J = 1$ [28] and 2 [48] singlet ungerade Rydberg levels mixed also by rotational coupling. The study was extended here to higher J levels and also to predissociated levels, for which an average or a more detailed study was necessary, and it produced very good results.

ACKNOWLEDGMENTS

We acknowledge the Helmholtz-Zentrum Berlin–Electron Storage Ring BESSY II for providing synchrotron radiation at beamline U125/2-10m-NIM, and we would like to thank Gerd Reichardt and Andreas Balzer for their assistance. The research leading to these results has received funding from the European Community’s Seventh Framework Programme (FP7/2007-2013) under Grant Agreement No. 226716. A.K. would like to acknowledge the Otto-Braun-Fonds of the University of Kassel for financial support.

-
- [1] J. J. Hopfield, *Nature (London)* **125**, 927 (1930).
 [2] T. Namioka, *J. Chem. Phys.* **41**, 2141 (1964).
 [3] A. Monfils, *J. Mol. Spectrosc.* **15**, 265 (1965).
 [4] S. Takezawa, *J. Chem. Phys.* **52**, 2575 (1970).
 [5] G. Herzberg and Ch. Jungen, *J. Mol. Spectrosc.* **41**, 425 (1972).
 [6] M. Glass-Maujean, J. Breton, and P. M. Guyon, *Chem. Phys. Lett.* **63**, 591 (1979).
 [7] P. M. Dehmer and W. A. Chupka, *Chem. Phys. Lett.* **70**, 127 (1980).
 [8] M. Glass-Maujean, J. Breton, and P. M. Guyon, *Chem. Phys. Lett.* **112**, 25 (1984).
 [9] P. S. Julienne, *Chem. Phys. Lett.* **8**, 27 (1971).
 [10] F. Fiquet-Fayard and O. Gallais, *Mol. Phys.* **20**, 527 (1971); *Chem. Phys. Lett.* **16**, 18 (1972).
 [11] H. Gao, Ch. Jungen, and C. H. Greene, *Phys. Rev. A* **47**, 4877 (1993).
 [12] Ch. Jungen and S. C. Ross, *Phys. Rev. A* **55**, R2503 (1997).
 [13] M. Glass-Maujean, Ch. Jungen, H. Schmoranzer, A. Knie, I. Haar, R. Hentges, W. Kielich, K. Jänkälä, and A. Ehresmann, *Phys. Rev. Lett.* **104**, 183002 (2010).
 [14] M. Glass-Maujean, Ch. Jungen, G. Reichardt, A. Balzer, H. Schmoranzer, A. Ehresmann, I. Haar and P. Reiss, *Phys. Rev. A* **82**, 062511 (2010).
 [15] U. Fano, *Nuovo Cimento* **12**, 154 (1935); *Phys. Rev.* **124**, 1866 (1961).
 [16] H. Beutler, A. Deubner, and H. Jünger, *Z. Naturforsch.* **98**, 181 (1935).
 [17] J. Breton, P. M. Guyon, and M. Glass-Maujean, *Phys. Rev. A* **21**, 1909 (1980).
 [18] M. Glass-Maujean, J. Breton, B. Thièblemont, and K. Ito, *Phys. Rev. A* **32**, 947 (1985).
 [19] M. Glass-Maujean, Ch. Jungen, M. Roudjane, and W.-Ü. L. Tchang-Brillet, *J. Chem. Phys.* **134**, 204305 (2011).
 [20] L. Wolniewicz, T. Orlikowski, and G. Staszewska, *J. Mol. Spectrosc.* **238**, 118 (2006); http://www.fizyka.umk.pl/ftp/publications/ifiz/luwo/B6P4_06.zip.
 [21] G. D. Dickenson, T. I. Ivanov, M. Roudjane, N. de Oliveira, D. Joyeux, L. Nahon, W.-Ü. L. Tchang-Brillet, M. Glass-Maujean, I. Haar, A. Ehresmann, and W. Ubachs, *J. Chem. Phys.* **133**, 144317 (2010).
 [22] G. D. Dickenson, T. I. Ivanov, W. Ubachs, M. Roudjane, N. de Oliveira, D. Joyeux, L. Nahon, W.-Ü. L. Tchang-Brillet, M. Glass-Maujean, H. Schmoranzer, A. Knie, S. Kübler, and A. Ehresmann, *Mol. Phys.* **109**, 2693 (2011).
 [23] J. A. Beswick and M. Glass-Maujean, *Phys. Rev. A* **35**, 3339 (1987).
 [24] F. Mrugala, *Mol. Phys.* **65**, 377 (1988).
 [25] Ch. Jungen, *Phys. Rev. Lett.* **53**, 2394 (1984).
 [26] M. Glass-Maujean and Ch. Jungen, *J. Phys. Chem. A* **113**, 13124 (2009).
 [27] M. Glass-Maujean, Ch. Jungen, H. Schmoranzer, I. Haar, A. Knie, P. Reiss, and A. Ehresmann, *J. Phys. Chem.* **135**, 144302 (2011).
 [28] M. Glass-Maujean, H. Schmoranzer, I. Haar, A. Knie, P. Reiss, and A. Ehresmann, *J. Phys. Chem.* **136**, 134301 (2012).
 [29] L. Wolniewicz and G. Staszewska, *J. Mol. Spectrosc.* **220**, 45 (2003); http://www.fizyka.umk.pl/ftp/publications/ifiz/luwo/1Pi_u.02.
 [30] Ch. Jungen and O. Atabek, *J. Chem. Phys.* **66**, 5584 (1977).
 [31] K. Dressler, R. Gallusser, P. Quadrelli, and L. Wolniewicz, *J. Mol. Spectrosc.* **75**, 205 (1979).
 [32] M. Roudjane, F. Launay, and W.-Ü. L. Tchang-Brillet, *J. Chem. Phys.* **125**, 214305 (2006).
 [33] C. H. Greene and Ch. Jungen, *Adv. At. Mol. Phys.* **21**, 51 (1985).
 [34] *Molecular Applications of Quantum Defect Theory*, edited by Ch. Jungen (Institute of Physics, Bristol, 1996).

- [35] G. Staszewska and L. Wolniewicz, *J. Mol. Spectrosc.* **212**, 208 (2002); see also <http://www.fizyka.umk.pl/ftp/publications/ifiz/luwo/>.
- [36] G. Staszewska and L. Wolniewicz, *J. Mol. Spectrosc.* **217**, 181 (2003); see also <http://www.fizyka.umk.pl/ftp/publications/ifiz/luwo/>.
- [37] L. Wolniewicz, *J. Chem. Phys.* **99**, 1851 (1993).
- [38] M. Glass-Maujean, P. Quadrelli, and K. Dressler, *J. Chem. Phys.* **80**, 4355 (1984).
- [39] H. Wind, *J. Chem. Phys.* **42**, 2371 (1965).
- [40] D. M. Bishop and R. W. Wetmore, *Mol. Phys.* **26**, 145 (1973); **27**, 279 (1974).
- [41] L. Wolniewicz and T. Orlikowski, *Mol. Phys.* **74**, 103 (1991).
- [42] M. Glass-Maujean, S. Klumpp, L. Werner, A. Ehresmann, and H. Schmoranzer, *J. Chem. Phys.* **126**, 144303 (2007).
- [43] M. Glass-Maujean, S. Klumpp, L. Werner, A. Ehresmann, and H. Schmoranzer, *Mol. Phys.* **105**, 1535 (2007).
- [44] M. Glass-Maujean, S. Klumpp, L. Werner, A. Ehresmann, and H. Schmoranzer, *J. Mol. Spectrosc.* **249**, 51 (2008).
- [45] M. Glass-Maujean, S. Klumpp, L. Werner, A. Ehresmann, and H. Schmoranzer, *J. Chem. Phys.* **128**, 094312 (2008).
- [46] G. Reichardt, J. Bahrdt, J.-S. Schmidt, W. Gudat, A. Ehresmann, R. Müller-Albrecht, H. Molter, H. Schmoranzer, M. Martins, N. Schwentner, and S. Sasaki, *Nucl. Instrum. Methods Phys. Res., Sect. A* **467–468**, 462 (2001).
- [47] H. Abgrall, E. Roueff, F. Launay, and J.-Y. Roncin, *Can. J. Phys.* **72**, 856 (1994); <http://amrel.obspm.fr/molat/index.php?page=pages/Molecules/H2/H2can94.php>.
- [48] M. Glass-Maujean, H. Schmoranzer, I. Haar, A. Knie, P. Reiss, and A. Ehresmann, *J. Chem. Phys.* **137**, 084303 (2012).